

Tempered fractional Brownian motion on finite intervals

Thomas Vojta ^{a,1}, Zachary Miller ^{b,1}, Samuel Halladay ^{c,1,2}

¹Department of Physics, Missouri University of Science and Technology, Rolla, Missouri 65409, USA

²Department of Applied Physics, Yale University, New Haven, Connecticut 06520, USA

Received: date / Accepted: date

Abstract Diffusive transport in many complex systems features a crossover between anomalous diffusion at short times and normal diffusion at long times. This behavior can be mathematically modeled by cutting off (tempering) beyond a mesoscopic correlation time the power-law correlations between the increments of fractional Brownian motion. Here, we investigate such tempered fractional Brownian motion confined to a finite interval by reflecting walls. Specifically, we explore how the tempering of the long-time correlations affects the strong accumulation and depletion of particles near reflecting boundaries recently discovered for untempered fractional Brownian motion. We find that exponential tempering introduces a characteristic size for the accumulation and depletion zones but does not affect the functional form of the probability density close to the wall. In contrast, power-law tempering leads to more complex behavior that differs between the superdiffusive and subdiffusive cases.

1 Introduction

Diffusive transport phenomena can be found in a wide variety of fields such as physics, chemistry, biology, and beyond. According to Einstein [1], Langevin [2], and Smoluchowski [3], diffusion arises from the motion of the particles in question being stochastic. It is often characterized in terms of the power-law relation $\langle x^2 \rangle \sim t^\alpha$ between the mean-square displacement $\langle x^2 \rangle$ of a diffusing particle and the elapsed time t . The exponent value $\alpha = 1$ corresponds to normal diffusion which emerges naturally if the stochastic motion is local in

time and space [4]. Recently, there has been significant interest in stochastic motion with $\alpha \neq 1$, i.e., in anomalous diffusion [5, 6]. Depending on the value of the anomalous diffusion exponent α , one can distinguish subdiffusion ($0 < \alpha < 1$) for which $\langle x^2 \rangle$ grows slower than t and superdiffusion ($1 < \alpha < 2$) for which $\langle x^2 \rangle$ grows faster than t . Both subdiffusion and superdiffusion have been observed experimentally in numerous systems (see. e.g. Ref. [7–12] and references therein), in part because modern microscopy provides unprecedented information about the motion of single molecules in complex environments [13–15].

Anomalous diffusion can arise if the random motion violates the condition of locality in time and space, e.g., when individual displacements (steps) of the diffusing particle are long-range correlated in time. Fractional Brownian motion (FBM) is a paradigmatic mathematical model of this situation. It was first introduced by Kolmogorov [16] and later explored by Mandelbrot and van Ness [17]. FBM is a self-similar Gaussian stochastic process with long-time (power-law) correlated increments which are antipersistent (anticorrelated) in the subdiffusive regime, $0 < \alpha < 1$, but persistent (positively correlated) in the superdiffusive regime $1 < \alpha < 2$. In the marginal case, $\alpha = 1$, FBM is identical to normal Brownian motion with uncorrelated increments. FBM processes have been used to describe the motion inside biological cells [18–23], the patterns of serotonergic fibers in vertebrate brains [24, 25], polymer dynamics [26, 27], electronic network traffic [28], as well as fluctuations of financial markets [29, 30].

Even though FBM has been explored quite extensively in mathematical literature (see, e.g., Refs. [31–34]), much of its behavior in confined geometries remains elusive because a generalized diffusion equation for FBM has yet to be found. Additionally, the method

^ae-mail: vojtat@mst.edu

^be-mail: zamydm@mst.edu

^ce-mail: samuel.halladay@yale.edu

of images [6, 35], often invoked for boundary value problems, fails. Existing results concern the first-passage problem on a semi-infinite interval [36–39]) and two-dimensional wedge and parabolic domains [40, 41]. In addition, properties of FBM close to an absorbing boundary were investigated in Refs. [42–48].

Recently, reflected FBM has attracted significant attention because the interplay between the long-time correlations and the reflecting barriers modifies the probability density function $P(x, t)$ of the diffusing particles. In the case of superdiffusive FBM, particles accumulate at the barrier whereas they are depleted near the barrier for subdiffusive FBM. More specifically, on a semi-infinite interval with a reflecting wall at the origin, P becomes highly non-Gaussian and develops a power-law singularity, $P \sim x^\kappa$, at the wall [49, 50]. On a finite interval with reflecting walls at both ends, the stationary probability density deviates from the uniform distribution found for normal diffusion [51] and also features power-law singularities at the walls [52]. Analogous results were obtained in higher dimensions [52].

In many of the experimental systems that feature anomalous diffusion, the anomalous power law $\langle x^2 \rangle \sim t^\alpha$ with $\alpha \neq 1$ does not extend to arbitrarily long times but eventually crosses over to normal diffusion ($\alpha = 1$) when the time exceeds a characteristic correlation time. To model this crossover, Molina-Garcia et al. [53] introduced the notion of tempered FBM, a stochastic process in which the long-time power-law correlations are cutoff beyond the tempering time t_* .¹ As the unusual behavior of the probability density of reflected FBM stems from the interplay of the reflecting barriers and the long-time correlations, it is important to ask how the tempering of these correlations affects the probability density.

Here, we therefore study the behavior of tempered FBM that is confined to a finite interval by reflecting walls at both ends. We employ large-scale computer simulations to study the mean-square displacement as well as the probability density function for hard exponential tempering of the correlations as well as softer power-law tempering. We distinguish the superdiffusive and subdiffusive regimes and compare our findings to the corresponding behavior of untempered FBM.

Our paper is organized as follows. We introduce FBM and tempered FBM in Sec. 2. Section 3 briefly summarizes key properties of (untempered) FBM with reflecting walls for later comparison with the tempered

case. Simulation results for exponentially tempered FBM on a finite interval with reflecting walls at both ends are presented in Sec. 4 whereas the corresponding results for power-law tempering are shown in Sec. 5. We conclude in Sec. 6.

2 Fractional Brownian motion and tempered fractional Brownian motion

2.1 Definition of fractional Brownian motion

We start from the definition of FBM as a continuous-time centered Gaussian stochastic process. Consider a particle located at position $X = 0$ at time $t = 0$. The covariance function of its position X at later times s and t is given by

$$\langle X(s)X(t) \rangle = K(s^\alpha - |s - t|^\alpha + t^\alpha) \quad (1)$$

where the exponent α is in the range $0 < \alpha < 2$. Setting $s = t$ results in a mean-square displacement of $\langle X^2 \rangle = 2Kt^\alpha$, i.e., the particle undergoes anomalous diffusion, with α playing the role of the anomalous diffusion exponent.

In preparation of the computer simulations, we now discretize time, $t_n = \epsilon n$, and define positions $x_n = X(t_n)$. Here, ϵ is the time step, and n is an integer. The resulting discrete version of FBM [55] can be understood as a random walk with identically Gaussian distributed and long-time correlated steps. The particle position x_n now evolves according to the recursion relation

$$x_{n+1} = x_n + \xi_n . \quad (2)$$

Here, the increments ξ_n constitute a discrete fractional Gaussian noise, a stationary Gaussian process of zero mean, variance $\sigma^2 = 2K\epsilon^\alpha$, and covariance

$$C_n^{\text{FBM}} = \langle \xi_m \xi_{m+n} \rangle = \frac{1}{2} \sigma^2 (|n+1|^\alpha - 2|n|^\alpha + |n-1|^\alpha) . \quad (3)$$

The covariance is positive (persistent) for $\alpha > 1$ and negative (anti-persistent) for $\alpha < 1$ (and $n \neq 0$). If $\alpha = 1$, the covariance vanishes for all $n \neq 0$ leading to an uncorrelated random walk, i.e., normal Brownian motion. In the long-time limit $n \rightarrow \infty$, the covariance follows the power-law form $\langle \xi_m \xi_{m+n} \rangle \sim \alpha(\alpha-1)|n|^{\alpha-2}$.

The time discretization error becomes unimportant if the time step ϵ is small compared to the considered times t . Equivalently, the individual step size σ needs to be small compared to the considered distances or system sizes. This continuum limit can be reached either by taking the time step ϵ to zero at fixed total time t

¹A different type of tempering was proposed by Meerschaert and Sabzikar [54]. It leads to fundamentally different behavior and does not describe the anomalously to normal diffusion crossover. We will briefly come back to this point in the concluding section.

or, equivalently, by taking t to infinity at fixed ϵ . We will follow the latter route by setting $\epsilon = \text{const}$ and considering long times $t \rightarrow \infty$.

2.2 Tempering the correlations

To model the crossover between anomalous diffusion and normal diffusion that is observed in many experimental systems, we now follow Ref. [53] and introduce a tempering (truncation) of the long-range correlations encoded in the covariance (3) of the fractional Gaussian noise. We will consider both a “hard” exponential tempering and a “softer” power-law tempering.

In the case of exponential tempering, the noise covariance (3) gets replaced by

$$C_n = C_n^{\text{FBM}} \exp(-|t_n|/t_*) \quad (4)$$

where t_* is the tempering (crossover) time scale governing the crossover from anomalous diffusion for times less than t_* to normal diffusion on time scales larger than t_* . For power-law tempering, the noise covariance reads

$$C_n = C_n^{\text{FBM}} (1 + |t_n|/t_*)^{-\mu}. \quad (5)$$

It is characterized by a positive decay exponent μ in addition to the tempering time t_* . Note that the Fourier transform $\tilde{C}(\omega)$ of the covariance C_n must be nonnegative because it represents the power spectrum of the noise ξ_n . Both (4) and (5) fulfill this condition as was demonstrated in Ref. [53] and verified numerically in our simulations.

Exponentially tempered fractional Gaussian noise with $\alpha = 1.2$ (in the superdiffusive regime) is illustrated in Fig. 1. Panel (a) shows how the power-law correlations are truncated beyond the tempering time. The corresponding noise power spectra in panel (b) are indeed nonnegative and feature crossovers from the FBM power law $\tilde{C} \sim \omega^{1-\alpha}$ at higher frequencies to $\tilde{C} = \text{const}$ at lower frequencies when the noise becomes effectively uncorrelated. Figure 2(a) illustrates the negative (anti-persistent) covariance for $\alpha = 0.8$ (in the subdiffusive regime). The corresponding Fourier transforms $\tilde{C}(\omega)$, shown in Fig. 2(b) for several tempering times, cross over from $\tilde{C} \sim \omega^{1-\alpha}$ to $\tilde{C} = \text{const}$ just as in the superdiffusive case.

The effects of power-law tempering are more complex than those of exponential tempering, and they differ between the superdiffusive and subdiffusive regimes. Let us first consider superdiffusive FBM ($1 < \alpha < 2$). In the presence of power-law tempering, the asymptotic large- n behavior of the noise covariance (5) is given by $C_n \sim |n|^{\alpha-2-\mu}$. If $\alpha - 2 - \mu > -1$ (called “weak

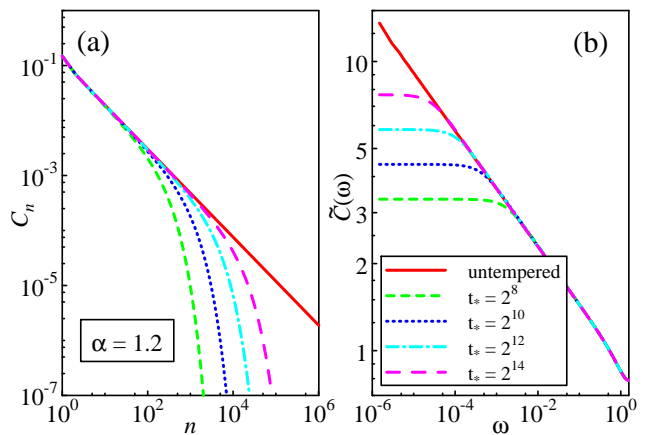


Fig. 1 (a) Covariance C_n of exponentially tempered fractional Gaussian noise with $\alpha = 1.2$ for different values of the tempering time t_* . (b) Corresponding Fourier transforms $\tilde{C}(\omega)$, representing the power spectra of the noise.

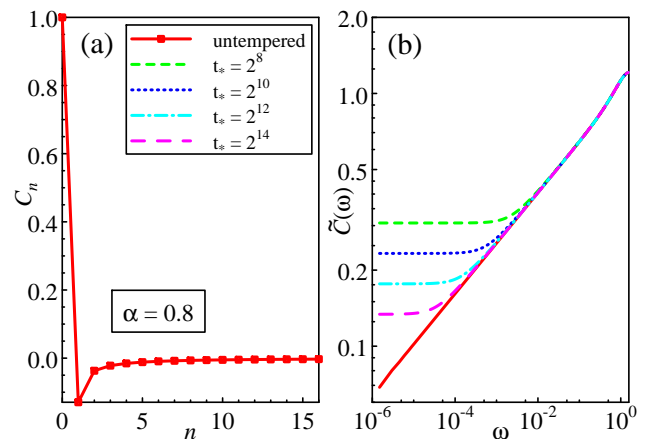


Fig. 2 (a) Covariance C_n of exponentially tempered fractional Gaussian noise with $\alpha = 0.8$ for different values of the tempering time t_* . The time axis in the plot is restricted to $n \leq 15$ to make the negative (anti) correlations clearly visible. For these n , the curves for all studied tempering times t_* coincide. (b) Corresponding Fourier transforms $\tilde{C}(\omega)$, representing the power spectra of the noise.

power-law tempering” in Ref. [53]), the Fourier transform $\tilde{C}(\omega)$ of the covariance diverges as $\tilde{C} \sim \omega^{1-\alpha+\mu}$ for $\omega \rightarrow 0$ implying that the power-law correlations are still relevant [see Fig. 3(a)]. If $\alpha - 2 - \mu < -1$ (called “strong power-law tempering” in Ref. [53]), the Fourier transform $\tilde{C}(\omega)$ of the covariance approaches a constant for $\omega \rightarrow 0$ as in the case of uncorrelated disorder.

Let us now turn to the subdiffusive case ($0 < \alpha < 1$). The Fourier transform $\tilde{C}(\omega)$ of untempered fractional Gaussian noise vanishes for $\omega \rightarrow 0$ in this regime, reflecting the perfect anticorrelations, $\sum_n C_n = 0$, of the noise. As any tempering destroys this equality (unless $\sum_n C_n$ is fine tuned to zero), the power spectra of the tempered noise contain an uncorrelated component re-

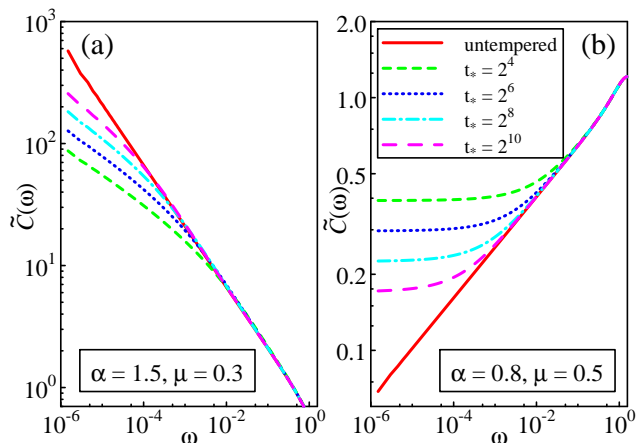


Fig. 3 Power spectrum $\tilde{C}(\omega)$ of power-law tempered fractional Gaussian noise for different values of the tempering time t_* . (a) $\alpha = 1.5$ and $\mu = 0.3$ (b) $\alpha = 0.8$ and $\mu = 0.5$.

flected in the nonzero low-frequency limit of the Fourier transform $\tilde{C}(\omega)$, see Fig. 3(b).

2.3 Reflecting boundaries

Reflecting boundaries that confine the motion of the diffusing particle can be introduced by modifying the recursion (2). The fractional Gaussian noise ξ_n defining the increments is understood as externally given [56]; it is therefore not modified by the barriers. Different implementations of the reflecting boundary conditions and their effects on FBM were studied in Ref. [52]. This paper demonstrated that details of the wall implementation are unimportant in the continuum limit. They influence the behavior only in a narrow spatial region close to wall (whose size is controlled by the step size σ).

Here, we define a reflecting boundary at position w that restricts the motion to $x \geq w$ by means of the recursion

$$x_{n+1} = \begin{cases} x_n + \xi_n & \text{if } x_n + \xi_n \geq w \\ x_n & \text{otherwise} \end{cases}. \quad (6)$$

In other words, the particle does not move at all if the step would take it into the forbidden region $x < w$. A reflecting boundary that restricts the motion to $x \leq w$ can be defined analogously.

2.4 Simulation details

In our computer simulations we investigate both exponentially and power-law tempered FBM on a finite interval of length L with reflecting walls at both ends. We use anomalous diffusion exponents α ranging from

0.6 (in the subdiffusive regime) to 1.6 (in the superdiffusive regime). The time step is set to $\epsilon = 1$ and $K = 1/2$ which fixes the variance of the individual increments at unity, $\sigma^2 = 1$.

Each simulation employs a large number of particles (between 20,000 and more than 10^6), leading to small statistical errors (characteristic errors will be given in some of the figure captions). Each particle carries out up to $2^{26} \approx 6.7 \times 10^7$ time steps. These long simulation times allow us to reach the continuum limit for which the time discretization becomes unimportant, as was explained in Sec. 2.1. Consequently, we select interval lengths that fulfill the condition $L/\sigma \gg 1$. Specifically, the interval lengths range from $L = 500$ for the most subdiffusive α to $L = 10^5$ for the most superdiffusive α values.

The fractional Gaussian noise, i.e., the increments ξ_n , are precalculated before each simulation run using the Fourier-filtering technique [57]. This method starts from a sequence of independent Gaussian random numbers χ_i of zero mean and unit variance (which are created via the Box-Muller transformation from random numbers produced by the LFSR113 [58] and KISS 2005 [59]) random number generators. The Fourier transform $\tilde{\chi}_\omega$ of these numbers is then converted via $\tilde{\xi}_\omega = [\tilde{C}(\omega)]^{1/2} \tilde{\chi}_\omega$, where $\tilde{C}(\omega)$ is the Fourier transform of the desired covariance function (4) or (5). The inverse Fourier transformation of the $\tilde{\xi}_\omega$ gives the desired noise values.

3 Review of fractional Brownian motion with reflecting walls

The behavior of (untempered) fractional Brownian motion in the presence of reflecting boundaries has recently attracted considerable attention because large-scale computer simulations have demonstrated that the interplay between the long-time correlations of FBM and the geometric confinement strongly affects the probability density of the diffusing particles.

In the case of FBM on the semi-infinite interval $(0, \infty)$ with a reflecting wall at the origin, particles accumulate close to the wall for superdiffusive FBM ($\alpha > 1$) whereas they are depleted at the wall for subdiffusive FBM ($\alpha < 1$) [49]. Specifically, the probability density function $P(x, t)$ of the particle position x at time t develops a power-law singularity, $P \sim x^\kappa$, for $x \rightarrow 0$. Based on extensive numerical data, Wada et al. [49] conjectured the relation $\kappa = 2/\alpha - 2$. Analogous results were found for biased FBM on a semi-infinite interval [50].

The properties of FBM confined to a finite interval by reflecting walls at both ends were studied in Ref.

[51]. The computer simulations showed that the stationary probability density depends on the value of the anomalous diffusion exponent α and differs from the flat distribution observed for normal diffusion. More specifically, the stationary probability density $P(x, L)$ on the interval $(-L/2, L/2)$ fulfills the scaling form

$$P(x, L) = \frac{1}{L} Y_\alpha(x/L) \quad (7)$$

in the continuum limit $L \gg \sigma$. Close to the left interval boundary, the α -dependent scaling function $Y_\alpha(z)$ develops a power-law singularity, $Y_\alpha(z) \sim (z + 1/2)^\kappa$ governed by the same exponent $\kappa = 2/\alpha - 2$ as the probability density on the semi-infinite interval [52]. The behavior near the right interval boundary is analogous.

We emphasize that the accumulation and depletion of the diffusing particles close to reflecting walls arise from the nonequilibrium nature of FBM. In contrast, the fractional Langevin equation, which is driven by the same fractional Gaussian noise as FBM but fulfills the fluctuation-dissipation theorem [60], reaches a thermal equilibrium stationary state. The corresponding probability density is governed by the Boltzmann distribution. This implies a flat probability density on a finite interval with reflecting walls, independent of the value of α , as was confirmed by computer simulations of the fractional Langevin equation [61].

We also note that there is an interesting similarity between the behavior of the probability density close to a reflecting wall (at position w), $P \sim |x - w|^{2/\alpha - 2}$, and the corresponding behavior close to an absorbing wall, $P \sim |x - w|^{2/\alpha - 1}$ [43, 44, 48].

4 Results: exponentially tempered fractional Brownian motion

In this section, we report the computer simulation results for exponentially tempered FBM, employing the noise covariance (4), on the interval $(-L/2, L/2)$ with reflecting boundaries at both ends. The particles start from the center of the interval, $x = 0$, at time $t = 0$. The simulations proceed until a steady state is reached, i.e., until the mean-square displacement, the probability density, and other quantities become time-independent.

To make contact with Ref. [53] where tempered FBM was introduced, we first discuss the time evolution of the mean-square displacement $\langle x^2 \rangle$. Figure 4 presents $\langle x^2 \rangle$ as a function of time t for the case of the superdiffusive anomalous diffusion exponent $\alpha = 1.5$ and several tempering times t_* . The data clearly reveal three different time regimes. Initially, for times small compared to the tempering time t_* , the mean-square displacement follows the same anomalous diffusion law

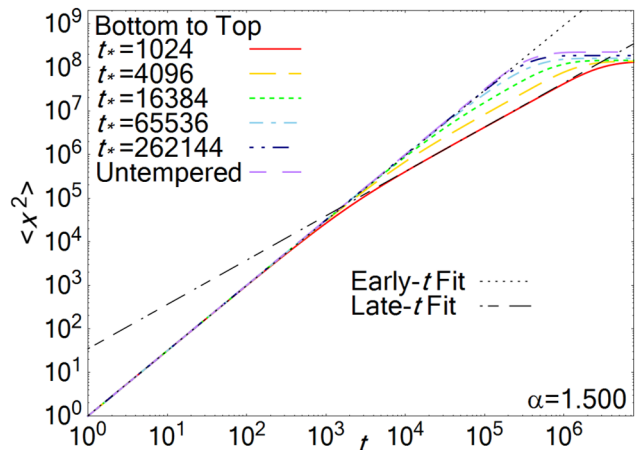


Fig. 4 Mean-square displacement $\langle x^2 \rangle$ vs. time t of exponentially tempered FBM for interval length $L = 40,000$, anomalous diffusion exponent $\alpha = 1.5$, and several values of the tempering time t_* . The data are averages over 1.2×10^6 particles. The resulting relative statistical error of $\langle x^2 \rangle$ is about 10^{-3} , well below the line width. The dotted line is a fit of the early-time behavior to $\langle x^2 \rangle \sim t^\alpha$ while the dash-dotted line is a fit to normal diffusion $\langle x^2 \rangle \sim t$.

$\langle x^2 \rangle \sim t^\alpha$ as untempered (and unconfined) FBM. When the time reaches t_* , the mean-square displacement undergoes a sharp crossover to normal diffusion $\langle x^2 \rangle \sim t$. Finally, $\langle x^2 \rangle$ saturates at a time-independent value indicating that a steady state has been reached. (Note that for a sufficiently large tempering time, $\langle x^2 \rangle$ may saturate before reaching the crossover to normal diffusion.) The properties of subdiffusive tempered FBM are completely analogous, as can be seen in Fig. 5 which presents the time evolution of the mean-square displacement for $\alpha = 0.667$. We have further confirmed this behavior by analyzing the cases $\alpha = 1.4, 1.2, 0.8$ and 0.6 .

In the following, we focus on the steady state reached at sufficiently long times and investigate its probability density function. Figure 6 presents an overview over the stationary probability density $P(x)$ for the (superdiffusive) anomalous diffusion exponent $\alpha = 1.5$ and several tempering times t_* . The data show that particles accumulate close to the wall for all tempering times. The width of the accumulation region decreases with decreasing tempering time because the long-time correlations responsible for the accumulation are cut off at a distance d_* from the wall, defined by $d_*^2 = 2Kt_*^\alpha$. For positions x outside of the accumulation region of width d_* , the stationary probability density is constant in agreement with the normal diffusion behavior at times beyond t_* . Analogous behavior is observed in the subdiffusive case $\alpha = 0.667$, as illustrated in Fig. 7. Here, particles are depleted close to the wall for all tempering

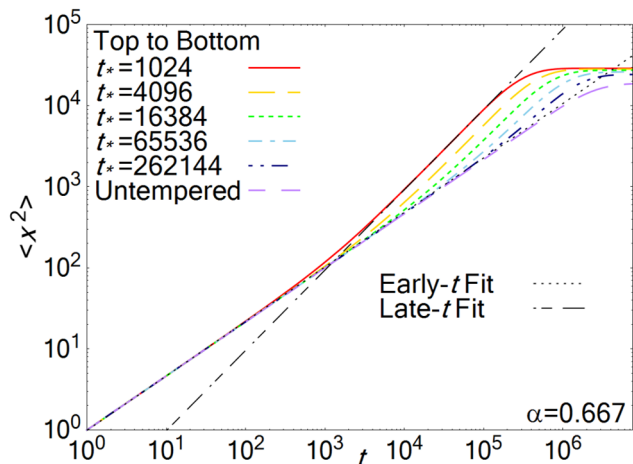


Fig. 5 Mean-square displacement $\langle x^2 \rangle$ vs. time t of exponentially tempered FBM for interval length $L = 600$, anomalous diffusion exponent $\alpha = 0.667$, and several values of the tempering time t_* . The data are averages over 1.2×10^6 particles. The dotted line is a fit of the early-time behavior to $\langle x^2 \rangle \sim t^\alpha$ while the dash-dotted line is a fit to normal diffusion $\langle x^2 \rangle \sim t$.

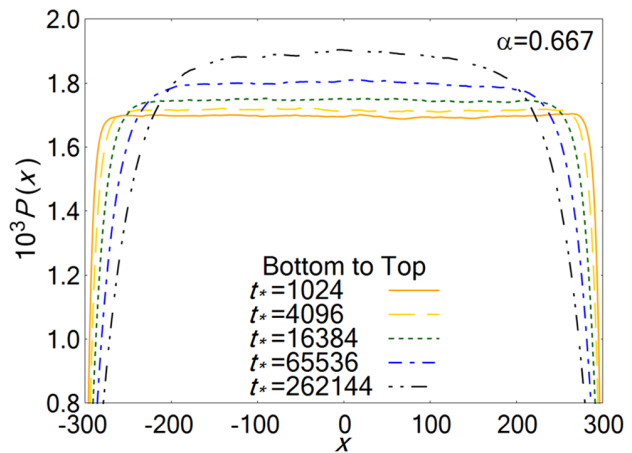


Fig. 7 Stationary probability density P vs. position x of exponentially tempered FBM for interval length $L = 600$, anomalous diffusion exponent $\alpha = 0.667$, and several values of the tempering time t_* . The data are averages over $2^{17} \approx 131,000$ time steps after the steady state has been reached for 1.2×10^6 particles.

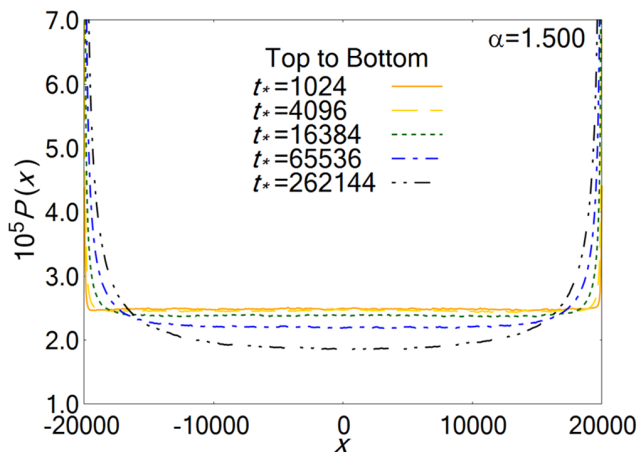


Fig. 6 Stationary probability density P vs. position x of exponentially tempered FBM for interval length $L = 40,000$, anomalous diffusion exponent $\alpha = 1.5$, and several values of the tempering time t_* . The data are averages over $2^{17} \approx 131,000$ time steps after the steady state has been reached for 1.2×10^6 particles. The resulting relative statistical error of P is about 10^{-3} .

times, and the width of the depletion region varies with t_* as above.

The emergence of the cutoff distance d_* as a new length scale suggests a generalization of the scaling form (7) for untempered FBM to the tempered case. The stationary probability density of exponentially tempered FBM with tempering time t_* on an interval of length L is expected to fulfill the scaling form

$$P(x, L, t_*) = \frac{1}{L} Z_\alpha(x/L, t_*^{\alpha/2}/L). \quad (8)$$

To verify that P fulfills this scaling form, we have performed simulations at fixed α for several interval lengths

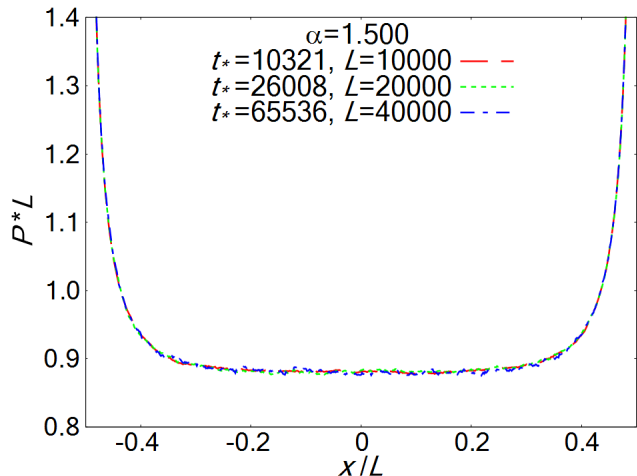


Fig. 8 Scaling plot of the stationary probability density of exponentially tempered FBM showing PL vs. position x/L for $\alpha = 1.5$. The interval lengths L and tempering times t_* have been chosen such that the second argument of the scaling function Z_α in eq. (8) stays constant. The data are averages over 2^{17} time steps for 1.2×10^6 particles.

and adjusted the tempering times such that the second argument of the scaling function Z_α stays constant. An example of this analysis is shown in Fig. 8 which confirms that the resulting stationary probability densities indeed collapse onto a single master curve when plotted as PL vs. x/L .

Let us now turn to the functional form of the stationary probability density close to the reflecting wall. As the probability density of untempered FBM develops a power-law singularity $P \sim (x - w)^\kappa$ with $\kappa = 2/\alpha - 2$ as function of the distance $x - w$ from the wall, we present in Fig. 9 a double-logarithmic plot (where

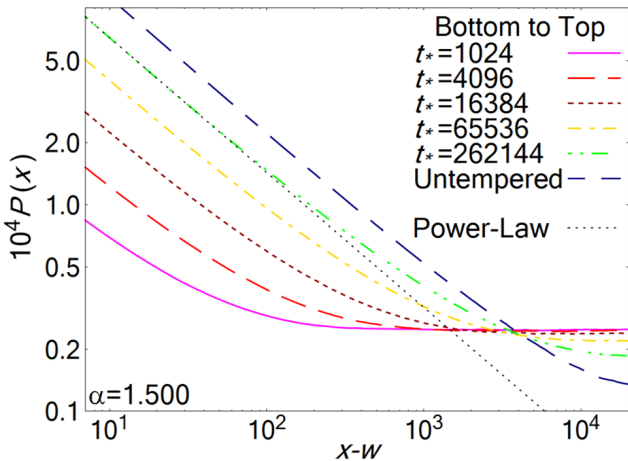


Fig. 9 Log-log plot of the stationary probability density P vs. the distance $x-w$ from the left reflecting wall ($w = -L/2$) for exponentially tempered FBM, interval length $L = 40,000$, anomalous diffusion exponent $\alpha = 1.5$, and several values of the tempering time t_* . The data are averages over 2^{17} time steps for 1.2×10^6 particles. The dotted line is a power-law fit $P \sim (x-w)^\kappa$ using the same exponent $\kappa = 2/\alpha - 2 = -2/3$ as applies to untempered FBM.

power-laws are represented by straight lines) of P near the left interval boundary ($w = -L/2$) vs. distance $x-w$ from the wall for $\alpha = 1.5$. The probability densities for all tempering times t_* display power-law behavior sufficiently close to the wall (for positions within their respective accumulation regions). The asymptotic behavior near the wall can be fitted well by the same power law, $P \sim (x-w)^\kappa$ with $\kappa = 2/\alpha - 2 = -2/3$, as holds for untempered FBM. (As all curves become parallel for small $x-w$, this power law holds for all t_* .) The behavior near the right interval boundary is completely analogous.

Figure 10 presents the same analysis for the subdiffusive case of $\alpha = 0.667$. It demonstrates that the stationary probability density behaves as a power-law, $P \sim (x-w)^\kappa$ with $\kappa = 2/\alpha - 2 = 1$, in the depletion region close to the wall for all tempering times.

5 Results: power-law tempered fractional Brownian motion

As explained in Sec. 2.2, the properties of power-law tempered FBM, characterized by the noise covariance (5), are more complex than those of exponentially tempered FBM. Moreover, superdiffusive and subdiffusive FBM are affected by the tempering in qualitatively different fashions.

Let us start with the superdiffusive case ($1 < \alpha < 2$). If the tempering exponent μ fulfills the inequality $\alpha - \mu > 1$ (weak power-law tempering), the mo-

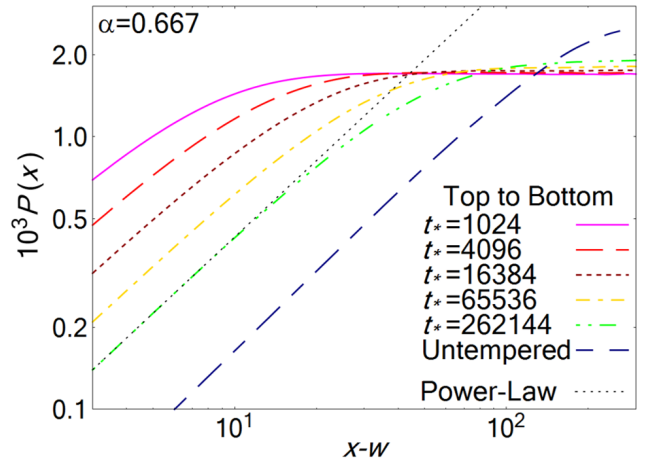


Fig. 10 Log-log plot of the stationary probability density P vs. the distance $x-w$ from the left reflecting wall ($w = -L/2$) for exponentially tempered FBM, interval length $L = 600$, anomalous diffusion exponent $\alpha = 0.667$, and several values of the tempering time t_* . The data are averages over 2^{17} time steps for 1.2×10^6 particles. The dotted line is a power-law fit $P \sim (x-w)^\kappa$ using the same exponent $\kappa = 2/\alpha - 2 = 1$ as applies to untempered FBM.

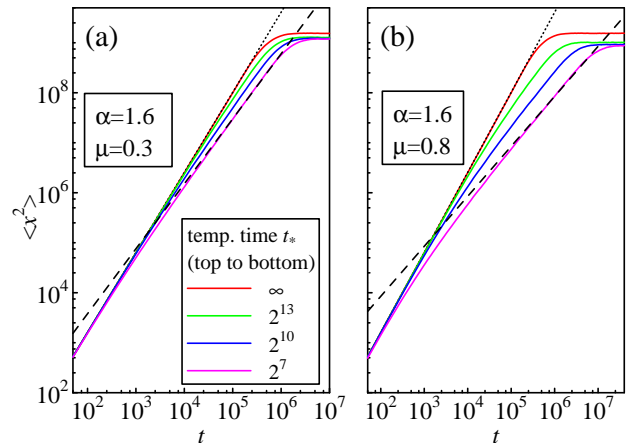


Fig. 11 Mean-square displacement $\langle x^2 \rangle$ vs. time t of power-law tempered FBM for interval length $L = 10^5$ and several values of the tempering time t_* . (a) Weak power-law tempering, $\alpha = 1.6$, $\mu = 0.3$. (b) Strong power-law tempering, $\alpha = 1.6$, $\mu = 0.8$. The data are averages over 20,000 particles. The resulting relative statistical error of $\langle x^2 \rangle$ is about 10^{-2} , well below the line width. The dotted lines are fits of the early-time behavior to $\langle x^2 \rangle \sim t^\alpha$. The dashed line is a fit to $\langle x^2 \rangle \sim t^{\alpha-\mu}$ in panel (a) while it represents a fit to normal diffusion $\langle x^2 \rangle \sim t$ in panel (b).

tion crosses over from anomalous diffusion governed by $\langle x^2 \rangle \sim t^\alpha$ at times $t \ll t_*$ to anomalous diffusion $\langle x^2 \rangle \sim t^{\alpha-\mu}$ for times $t \gg t_*$ [53]. The behavior of the mean-square displacement for weakly power-law tempered FBM on a finite interval is illustrated in Fig. 11(a) for $\alpha = 1.6$ and $\mu = 0.3$. The data demonstrate two distinct anomalous diffusion regimes with exponents α and $\alpha - \mu$ before the mean-square displacement

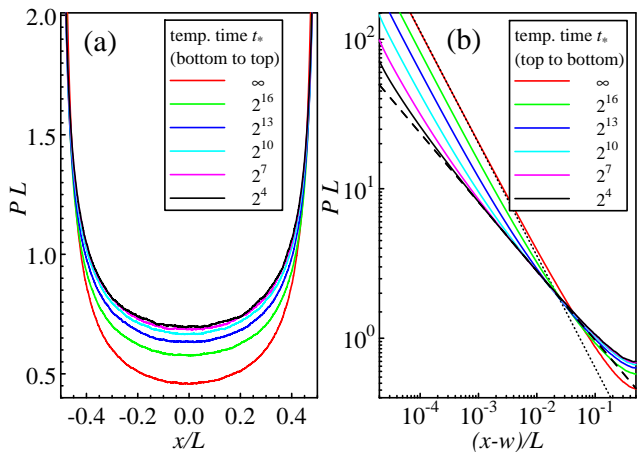


Fig. 12 (a) Scaled stationary probability density PL vs. scaled position x/L of power-law tempered FBM for interval length $L = 10^5$, anomalous diffusion exponent $\alpha = 1.6$, tempering exponent $\mu = 0.3$, and several values of the tempering time t_* . The data are averages over $2^{25} \approx 33$ million time steps after the steady state has been reached for 20,000 particles. (b) Log-log plot of the scaled stationary probability density PL vs. the scaled distance from the wall $(x-w)/L$. The dotted line is a power-law fit $P \sim (x-w)^\kappa$ of the untempered data using $\kappa = 2/\alpha - 2 = -0.75$. The dashed line is a power-law fit of the preasymptotic behavior for $t_* = 2^4$ using the exponent $\kappa = 2/(\alpha - \mu) - 2 \approx -0.462$.

saturates when the particles have spread over the interval. For strong power-law tempering ($\alpha - \mu < 1$), in contrast, the motion for times $t \gg t_*$ is normal diffusion. This can be seen in Fig. 11(b) which presents the mean-square displacement for $\alpha = 1.6$ and $\mu = 0.8$. Note that the crossover from anomalous to normal diffusion is much slower than in the case of exponential tempering, see Fig. 4.

We now discuss the stationary probability density for superdiffusive power-law tempered FBM on a finite interval. Figure 12(a) presents an overview of the stationary probability density for $\alpha = 1.6$ and $\mu = 0.3$, i.e., for a weak tempering situation. In contrast to the behavior of exponentially tempered FBM (see Fig. 6), the probability density does not become flat away from the reflecting walls, even for the shortest tempering time of only $t_* = 2^4$. This reflects the fact that the motion does not cross over to normal diffusion but remains superdiffusive beyond t_* . Figure 12(b) analyzes the functional form of the probability density P near the reflecting wall. The data demonstrate that P follows the power law $P \sim (x-w)^\kappa$ with $\kappa = 2/\alpha - 2$ asymptotically close to the wall. Outside the asymptotic region of width $d_* = (2Kt_*^\alpha)^{1/2}$, the behavior is governed by the anomalous diffusion exponent $\alpha - \mu$. Assuming that the condition $d_* \ll L$ is fulfilled, we therefore expect a well-defined preasymptotic region $d_* \ll x \ll L$ in which the probability density follows a power law $P \sim (x-w)^\kappa$,

but with exponent $\kappa = 2/(\alpha - \mu) - 2$. This behavior is indeed observed in Fig. 12(b).

We have performed an analogous analysis for the strongly power-law tempered case of $\alpha = 1.6$ and $\mu = 0.8$. In agreement with the fact that the motion crosses over to normal diffusion for times beyond t_* , the properties of the stationary probability density qualitatively resemble those of exponentially tempered FBM (Figs. 6 and 9) rather than those of weakly power-law tempered FBM. Specifically, P follows the power law $P \sim (x-w)^\kappa$ with $\kappa = 2/\alpha - 2$ asymptotically close to the wall, but outside of the asymptotic region of width d_* , the probability density approaches the constant behavior expected for normal diffusion. As in the case of the mean-square displacement [Fig. 11(b)], the crossover between the anomalous and normal diffusion regimes is much slower than in the exponentially tempered case.

So far, our discussion of power-law tempered FBM has focused on the superdiffusive case. We now turn to subdiffusive power-law tempered FBM. The discussion in Sec. 2.2 emphasized that the subdiffusive behavior of FBM with $\alpha < 1$ is the result of the perfect anticorrelations of the corresponding fractional Gaussian noise, encoded in the relation $\sum_n C_n = 0$ for the noise covariance. This is equivalent to a vanishing of the covariance Fourier component $\tilde{C}(0)$. These anticorrelations are fragile, however, as any modification of the noise covariance function generically leads to a violation of the relation $\sum_n C_n = 0$ unless the covariance is fine tuned. More specifically, the power-law tempered noise with covariance (5) violates the perfect anticorrelation condition for all μ and t_* . Consequently, power-law tempered subdiffusive FBM is expected to cross over from anomalous diffusion for times below t_* to normal diffusion at longer times.²

Figure 13(a) presents the time evolution of the mean-square displacement for $\alpha = 0.8$, $\mu = 0.5$ and several t_* ; the data confirm this expectation. The (scaled) stationary probability density for the same stochastic processes is presented in Fig. 13(b) which shows that the probability density P goes to zero at the reflecting wall, as in the untempered case. Power-law fits demonstrate that P follows the same asymptotic behavior, $P \sim (x-w)^\kappa$ with $\kappa = 2/\alpha - 2$ as in the untempered case. Outside the asymptotic region of width $d_* = (2Kt_*^\alpha)^{1/2}$, P approaches the constant behavior expected for normal diffusion.

²Naively, one might have expected a crossover between two anomalous diffusion regimes, characterized by anomalous diffusion exponent values α (for times below t_*) and $\alpha - \mu$ (for times above t_*). Because of the fragility of the anticorrelations in subdiffusive FBM, this is not the case.

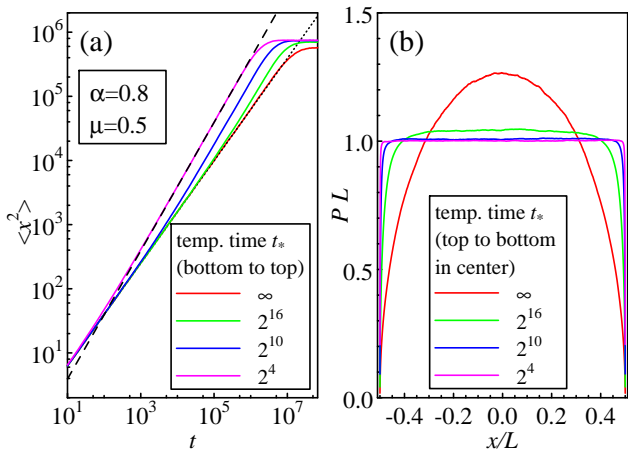


Fig. 13 (a) Mean-square displacement $\langle x^2 \rangle$ vs. time t of power-law tempered FBM for $\alpha = 0.8$, $\mu = 0.5$, interval length $L = 3000$ and several values of the tempering time t_* . The data are averages over 50,000 particles. The dotted line is a fit of the early-time behavior to $\langle x^2 \rangle \sim t^\alpha$. The dashed line is a fit of the behavior after t_* to normal diffusion $\langle x^2 \rangle \sim t$. (b) Scaled stationary probability density PL vs. scaled position x/L for the same parameters as in panel (a). The data are averages over $2^{25} \approx 33$ million time steps after the steady state has been reached.

6 Conclusions

In summary, we have employed large-scale computer simulations to study tempered FBM [53], a stochastic process with long-time power-law correlations that are cut off at some mesoscopic time scale, the tempering time t_* . Specifically, we have analyzed the behavior of tempered FBM confined to a finite one-dimensional interval by means of reflecting walls in order to understand how the tempering of the correlations affects the unusual accumulation and depletion effects recently observed for (untempered) reflected FBM.

The motion of particles that start at the center of the interval features three distinct time regimes (assuming the interval length is sufficiently large and/or the tempering time is sufficiently small). At times below t_* , the particles spread exactly as they would for untempered FBM. Beyond t_* , the particles continue to spread but the motion changes qualitatively due to the cutoff of the correlations. At the longest times, when the particles have spread over the entire interval, the particle distribution reaches a stationary state.

The character of the stochastic process beyond t_* depends on the type of the tempering. For a hard exponential cutoff of the correlations, the motion crosses over to normal diffusion. For the softer power-law tempering, the behavior is more complex and depends on the values of α and μ . The motion beyond t_* is of normal diffusion type if the underlying FBM is either superdiffusive with $\alpha - \mu < 1$ or subdiffusive (for any

subdiffusive α and $\mu > 0$). For superdiffusive power-law tempered FBM with $\alpha - \mu > 1$, in contrast, the motion beyond t_* is anomalous diffusion with a reduced anomalous diffusion exponent value of $\alpha - \mu$.

The main focus of the present paper has been on the stationary probability density that the stochastic process reaches after sufficiently long times. Our simulation results demonstrate that tempered FBM features the same accumulation and depletion effects close to a reflecting wall as untempered FBM. More specifically, particles accumulate near the wall in the superdiffusive case but are depleted at the wall in the subdiffusive case. Asymptotically close to the wall, the functional form of the stationary probability density of tempered FBM is governed by the same power-law singularity $P \sim (x - w)^\kappa$ with $\kappa = 2/\alpha - 2$ as untempered FBM ($x - w$ represents the distance from the wall). However, due to the cutoff of the correlations, this power-law behavior is restricted to a region of finite width $d_* = (2Kt_*^\alpha)^{1/2}$ near the wall. Outside of this region, the probability density becomes flat in the cases where the motion beyond t_* is of normal diffusion type. The most interesting case occurs for superdiffusive power-law tempered FBM with $\alpha - \mu > 1$. Here, the probability density features two power-law regimes with κ values $\kappa = 2/\alpha - 2$ (asymptotically close to the wall) and $\kappa = 2/(\alpha - \mu) - 2$ (for $d_* \ll |x - w| \ll L$).

We also found that the tempering of the correlations introduces the new length scale d_* and thus leads to the generalized scaling form (8) of the stationary probability density. Our numerical data fulfill this scaling form with high accuracy.

Let us now put our results into a broader perspective. In the present work we have considered tempered FBM confined to a finite interval by two reflecting walls. Instead, one could also consider a situation with only a single reflecting wall and introduce a bias (nonzero mean of the increments) towards the wall as was done for untempered FBM in Ref. [50]. We expect that the behavior of such a system close to the wall is qualitatively identical to the behavior found in the present paper.

It is also interesting to consider a generalized Langevin equation driven by the same tempered fractional Gaussian noise as the tempered FBM studied in the present paper [53]. A key question is whether the probability density of such a Langevin equation confined to a finite interval also shows accumulation and or depletion effects close to the confining walls. If the generalized Langevin equation fulfills the fluctuation-dissipation theorem (which connects the noise covariance and the damping kernel), the stationary state is expected to be a thermal equilibrium state which has a flat probabil-

ity density independent of the values of α and μ . (For the untempered fractional Langevin equation, this absence of accumulation and depletion effects was recently observed in simulations [61].) This highlights that the nonequilibrium nature of FBM (tempered or untempered) is responsible for the accumulation and depletion effects near a reflecting wall.

We emphasize that the notion of tempering the fractional Gaussian noise, as introduced in Ref. [53] and employed in the present paper, differs fundamentally from a model proposed by Meerschaert and Sabzikar [54] in which exponential tempering factors are introduced directly into Mandelbrot's definition [17] of FBM. That process does not describe the crossover from anomalous diffusion to normal diffusion. Instead, its mean-square displacement approaches a constant in the long-time limit, i.e., it describes a confined motion [53, 62]. A Langevin equation driven by the corresponding noise leads to ballistic long-time behavior, very different from the processes considered in the present paper.

Finally, we point out that the tempering of the correlations provides a powerful tool in applications in which a stochastic process is used to model experimental data. For example, FBM was recently put forward as a model to explain the spatial distribution of serotonergic fibers in vertebrate brains [24, 25]. Despite the limited "neurobiological input", the model captures important aspects of the highly nonuniform distributions of these fibers throughout the brain. Tempering will permit further refinements of the model to better represent the observed fiber densities. We expect similar advantages in many other applications.

Acknowledgements This work was supported in part by a Cottrell SEED award from Research Corporation and by the National Science Foundation under Grant Nos. DMR-1828489 and OAC-1919789. The simulations were performed on the Pegasus and Foundry clusters at Missouri S&T. We acknowledge helpful discussions with Ralf Metzler and Skirmantas Janušonis.

Author Contribution Statement T.V. conceived and coordinated the study. Z.M. and S.H. performed the computer simulations and analyzed the data. Z.M. and T.V. created the figures. T.V. wrote the manuscript.

References

1. A. Einstein, *Investigations on the Theory of the Brownian Movement* (Dover, New York, 1956).
2. P. Langevin, *C. R. Acad. Sci. Paris* **146**, 530 (1908).
3. M. von Smoluchowski, *Z. Phys. Chem.* **92U**, 129 (1918).
4. B. Hughes, *Random Walks and Random Environments, Volume 1: Random Walks* (Oxford University Press, Oxford, 1995).
5. J.-P. Bouchaud and A. Georges, *Physics Reports* **195**, 127 (1990).
6. R. Metzler and J. Klafter, *Physics Reports* **339**, 1 (2000).
7. F. Höfling and T. Franosch, *Rep. Progr. Phys.* **76**, 046602 (2013).
8. P. C. Bressloff and J. M. Newby, *Rev. Mod. Phys.* **85**, 135 (2013).
9. R. Metzler, J.-H. Jeon, A. G. Cherstvy, and E. Barkai, *Phys. Chem. Chem. Phys.* **16**, 24128 (2014).
10. Y. Meroz and I. M. Sokolov, *Physics Reports* **573**, 1 (2015).
11. R. Metzler, J.-H. Jeon, and A. Cherstvy, *Biochimica et Biophysica Acta* **1858**, 2451 (2016).
12. K. Nørregaard, R. Metzler, C. M. Ritter, K. Berg-Sørensen, and L. B. Oddershede, *Chemical Reviews* **117**, 4342 (2017).
13. X. S. Xie, P. J. Choi, G.-W. Li, N. K. Lee, and G. Lia, *Annual Review of Biophysics* **37**, 417 (2008).
14. C. Bräuchle, D. C. Lamb, and J. Michaelis, *Single Particle Tracking and Single Molecule Energy Transfer* (Wiley-VCH, Weinheim, 2012).
15. C. Manzo and M. F. Garcia-Parajo, *Rep. Progr. Phys.* **78**, 124601 (2015).
16. A. N. Kolmogorov, *C. R. (Doklady) Acad. Sci. URSS (N.S.)* **26**, 115 (1940).
17. B. B. Mandelbrot and J. W. V. Ness, *SIAM Review* **10**, 422 (1968).
18. J. Szymanski and M. Weiss, *Phys. Rev. Lett.* **103**, 038102 (2009).
19. M. Magdziarz, A. Weron, K. Burnecki, and J. Klafter, *Phys. Rev. Lett.* **103**, 180602 (2009).
20. S. C. Weber, A. J. Spakowitz, and J. A. Theriot, *Phys. Rev. Lett.* **104**, 238102 (2010).
21. J.-H. Jeon, V. Tejedor, S. Burov, E. Barkai, C. Selhuber-Unkel, K. Berg-Sørensen, L. Oddershede, and R. Metzler, *Phys. Rev. Lett.* **106**, 048103 (2011).
22. J.-H. Jeon, H. M.-S. Momme, M. Javanainen, and R. Metzler, *Phys. Rev. Lett.* **109**, 188103 (2012).
23. S. M. A. Tabei, S. Burov, H. Y. Kim, A. Kuznetsov, T. Huynh, J. Jureller, L. H. Philipson, A. R. Dinner, and N. F. Scherer, *Proc. Nat. Acad. Sci.* **110**, 4911 (2013).
24. S. Janušonis and N. Detering, *Biochimie* **161**, 15 (2019).
25. S. Janušonis, N. Detering, R. Metzler, and T. Vojta, *Front. Comp. Neuroscience* **14**, 56 (2020).
26. N. Chakravarti and K. Sebastian, *Chem. Phys. Lett.* **267**, 9 (1997).
27. D. Panja, *J. Stat. Mech.* **2010**, L02001 (2010).
28. T. Mikosch, S. Resnick, H. Rootzen, and A. Stegeman, *Ann. Appl. Probab.* **12**, 23 (2002).
29. F. Comte and E. Renault, *Math. Financ.* **8**, 291 (1998).
30. S. Rostek and R. Schöbel, *Econom. Model.* **30**, 30 (2013).
31. J.-P. Kahane, *Some Random Series of Functions* (Cambridge University Press, London, 1985).
32. A. M. Yaglom, *Correlation Theory of Stationary and Related Random Functions* (Springer, Heidelberg, 1987).
33. J. Beran, *Statistics for Long-Memory Processes* (Chapman & Hall, New York, 1994).
34. F. Biagini, Y. Hu, B. Øksendal, and T. Zhang, *Stochastic Calculus for Fractional Brownian Motion and Applications* (Springer, Berlin, 2008).
35. S. Redner, *A guide to first-passage processes* (Cambridge University Press, Cambridge, 2001).
36. A. Hansen, T. Engøy, and K. J. Måløy, *Fractals* **02**, 527 (1994).
37. M. Ding and W. Yang, *Phys. Rev. E* **52**, 207 (1995).
38. J. Krug, H. Kallabis, S. N. Majumdar, S. J. Cornell, A. J. Bray, and C. Sire, *Phys. Rev. E* **56**, 2702 (1997).
39. G. M. Molchan, *Commun. Math. Phys.* **205**, 97 (1999).

-
40. J.-H. Jeon, A. V. Chechkin, and R. Metzler, *EPL (Europhysics Letters)* **94**, 20008 (2011).
 41. F. Aurzada and M. A. Lifshits, *Theory Probab. Appl.* **64**, 490 (2019).
 42. C. Chatelain, Y. Kantor, and M. Kardar, *Phys. Rev. E* **78**, 021129 (2008).
 43. A. Zoia, A. Rosso, and S. N. Majumdar, *Phys. Rev. Lett.* **102**, 120602 (2009).
 44. K. J. Wiese, S. N. Majumdar, and A. Rosso, *Phys. Rev. E* **83**, 061141 (2011).
 45. M. Delorme and K. J. Wiese, *Phys. Rev. Lett.* **115**, 210601 (2015).
 46. M. Delorme and K. J. Wiese, *Phys. Rev. E* **94**, 012134 (2016).
 47. M. Arutkin, B. Walter, and K. J. Wiese, *Phys. Rev. E* **102**, 022102 (2020).
 48. T. Vojta and A. Warhover, *J. Stat. Mech.* **2021**, 033215 (2021).
 49. A. H. O. Wada and T. Vojta, *Phys. Rev. E* **97**, 020102 (2018).
 50. A. H. O. Wada, A. Warhover, and T. Vojta, *J. Stat. Mech.* **2019**, 033209 (2019).
 51. T. Guggenberger, G. Pagnini, T. Vojta, and R. Metzler, *New J. Phys.* **21**, 022002 (2019).
 52. T. Vojta, S. Halladay, S. Skinner, S. Janušonis, T. Guggenberger, and R. Metzler, *Phys. Rev. E* **102**, 032108 (2020).
 53. D. Molina-Garcia, T. Sandev, H. Safdari, G. Pagnini, A. Chechkin, and R. Metzler, *New J. Phys.* **20**, 103027 (2018).
 54. M. M. Meerschaert and F. Sabzikar, *Stat. Probab. Lett.* **83**, 2269 (2013).
 55. H. Qian, in *Processes with Long-Range Correlations: Theory and Applications*, edited by G. Rangarajan and M. Ding (Springer, Berlin, Heidelberg, 2003) pp. 22–33.
 56. Y. L. Klimontovich, *Statistical theory of open systems - Volume 1: A unified approach to kinetic description of processes in active systems* (Kluwer Academic Publishers, Dordrecht, 1995).
 57. H. A. Makse, S. Havlin, M. Schwartz, and H. E. Stanley, *Phys. Rev. E* **53**, 5445 (1996).
 58. P. L'Ecuyer, *Math. Comput.* **68**, 261 (1999).
 59. G. Marsaglia, “Double precision RNGs,” Posted to sci.math.num-analysis (2005), <http://sci.tech-archive.net/Archive/sci.math.num-analysis/2005-11/msg00352.html>.
 60. R. Kubo, *Rep. Progr. Phys.* **29**, 255 (1966).
 61. T. Vojta, S. Skinner, and R. Metzler, *Phys. Rev. E* **100**, 042142 (2019).
 62. Y. Chen, X. Wang, and W. Deng, *J. Stat. Phys.* **169**, 18 (2017).